Cosmic ray energy spectrum measurement with AMANDA

Ver. 0.2 Part 2

Dmitry Chirkin
chirkin@physics.berkeley.edu

University of California at Berkeley, USA

Talk outline

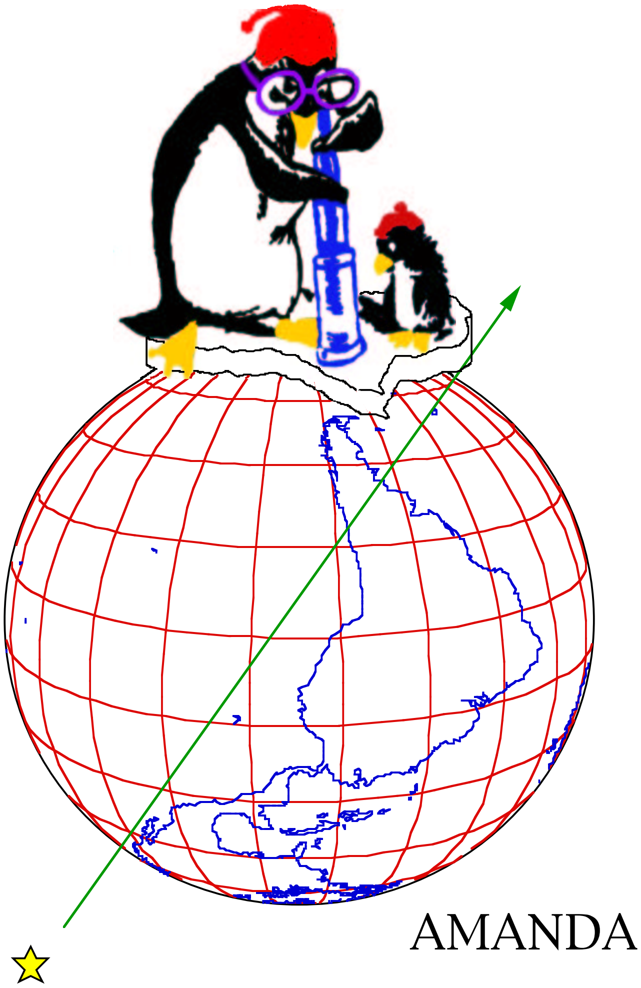

1. Better fit implementation.
2. Model of the N_{ch} behavior at small N_{ch}.
3. Fits for smaller energy (N_{ch}).
4. Summary of results.

Better fit implementation

The sum of two exponents fit is modified as follows:

$$f(x) = (e^{p_1+p_2\cdot x} + e^{p_3+p_4\cdot x}) \cdot \frac{1-\mathrm{erf}(\frac{p_5-x}{p_6})}{2}$$

This describes the behavior of N_{ch} distribution at low N_{ch} better and makes the fit almost independent of the region of the fit.

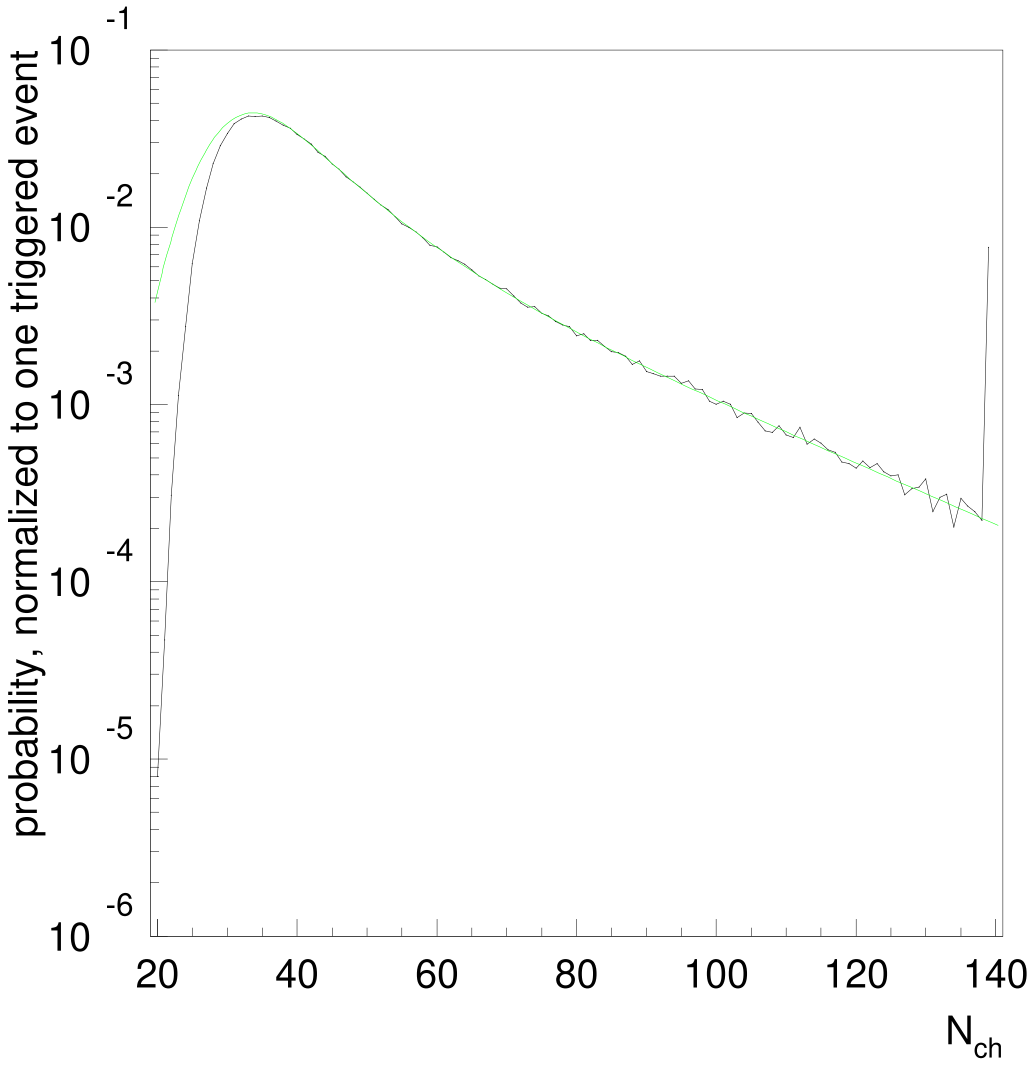

N_{ch} noise correction

The implementation of noise correction to N_{ch} has also changed. From the Zeuthen talk, an exponential distribution $P(n) = e^{a+b\cdot n}$ is modified by Poissonian noise $\frac{\lambda^n}{n!}e^{-\lambda}$ in the following way:

$$P_{tot}(n) = e^{a'+b\cdot n} \quad \text{with} \quad a' = a + \lambda(e^{-b} - 1)$$

$$a' \approx a - \lambda b$$

For slowly varying a and b this correction is varies from one point to another. However,

$$P_{tot}(n) = e^{a'+b\cdot n} = e^{a-\lambda b+b\cdot n} = e^{a+b\cdot(n-\lambda)} = P(n-\lambda)$$

Therefore, it is sufficient to shift the fit by λ to accommodate the noise correction.

Point of maximum slope change rate (N_{ms})

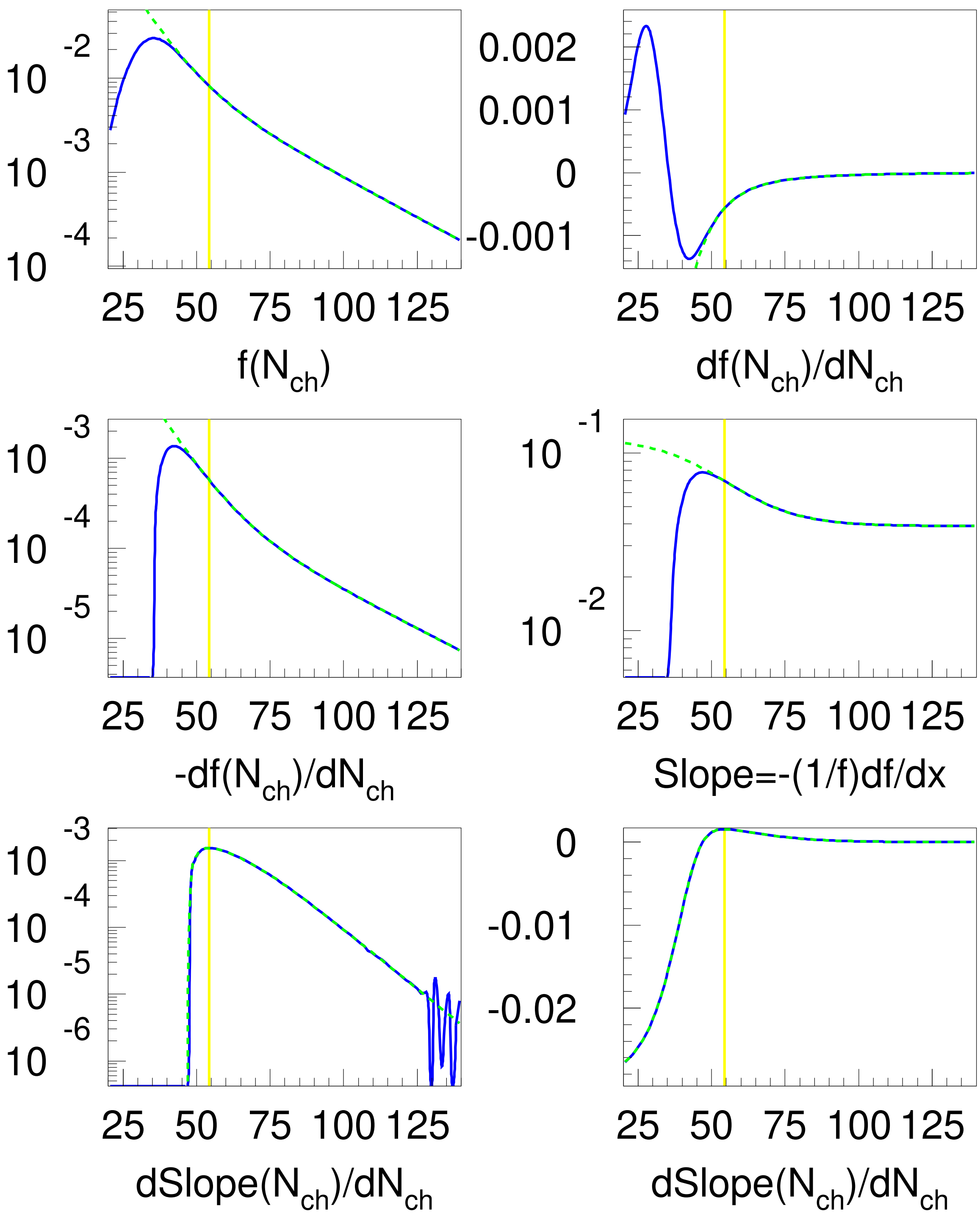

Slope of N_{ch} at N_{ms}: $Slope = -\frac{1}{f(N_{ch})} \cdot \frac{df(N_{ch})}{dN_{ch}}$

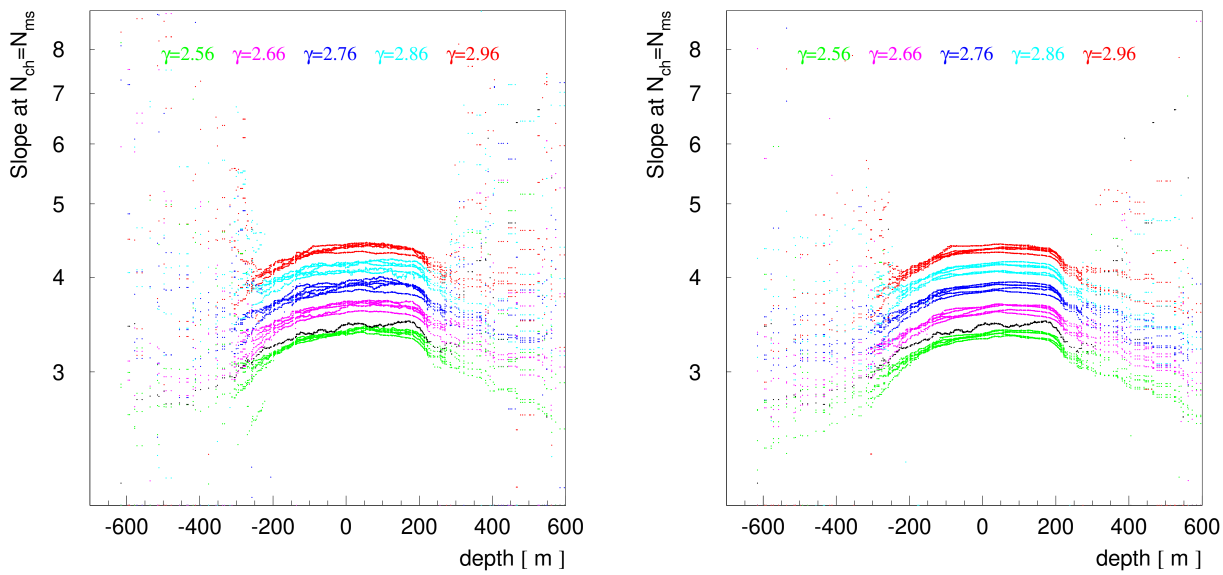

Number or events above N_{ms}:

$$Events = \int_{N_{ms}}^{N_{max}} f(x)dx$$

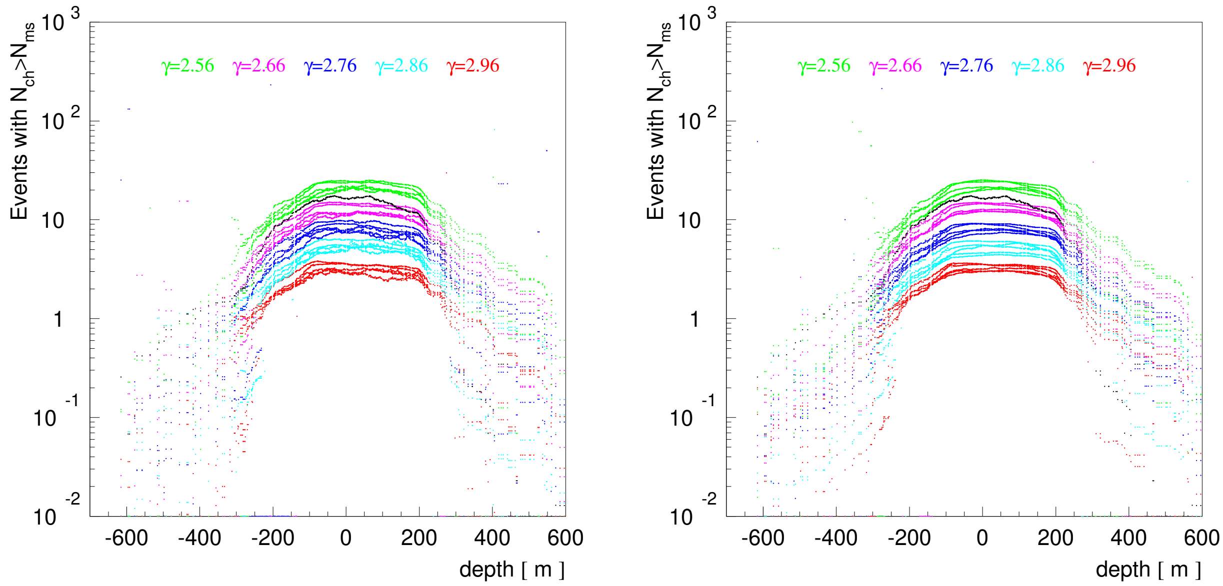

default no noise

Model of the N_{ch} behavior at small N_{ch}

From Part 1 (Zeuthen talk),

$$N(E_\mu) \approx \int_{+0}^{\infty} \left(1 - e^{-P(r)\cdot P_{ph}(E_{loss}(E_\mu))}\right) \frac{dN(r)}{dr} dr$$

For small N_{ch}, e.g. small $P_{ph}(E_{loss}(E_\mu))$,

$$N(E_\mu) \approx \int_{+0}^{\infty} P(r) \cdot P_{ph}(E_{loss}(E_\mu)) \frac{dN(r)}{dr} dr$$

Assuming that the OM depth density

$$\rho dh = \int_{+0}^{\infty} P(r) \frac{dN(r)}{dr} dr$$

is constant with depth h and introducing the depth h dependence of the muon energy E_μ, for a cylindrical detector located between depths h_1 and h_2 and a muon track going vertically down, we get

$$N = \int_{h_1}^{h_2} E_{loss}(h; E_\mu) \rho dh$$

In the above $P_{ph}(E)$ is assumed proportional to E, and coefficient of proportionality included into ρ.

Model of the N_{ch} behavior at small N_{ch}

Let E_μ be the muon energy at the surface. Then, solving the muon energy loss approximation equation $dE/dx = a + b \cdot E$ between $E_i = E(0)$ and $E_f = E(h)$, we get

$$\frac{dE}{dx}(h) = a + bE_f = (a + bE_i) \cdot e^{-bh}$$

Therefore,

$$N = (a + bE_i) \int_{h_1}^{h_2} e^{-bh} \rho dh$$

Depending on whether the muon stops inside the detector (at h, determined by $e^{bh} = 1 + bE_i/a$) or goes through, we get two solutions:

$$N = (a + bE_i) \cdot \frac{\rho}{b} \cdot \begin{cases} e^{-bh_1} - e^{-bh_2}, & 1 \\ e^{-bh_1} - \frac{1}{1+\frac{bE_i}{a}}, & 2 \end{cases}$$

$$N = \begin{cases} (a + bE_i) \cdot \frac{\rho}{b}(e^{-bh_1} - e^{-bh_2}) & = (a + bE_i) \cdot A \\ (a + bE_i) \cdot \frac{\rho}{b} e^{-bh_1} - \frac{\rho a}{b} & = (a + bE_i) \cdot B - C \end{cases}$$

Model of the N_{ch} behavior at small N_{ch}

Therefore, for a muon spectrum of $\Phi = \Phi_0 \cdot E^{-\gamma}$ at the surface, one gets

$$\Phi = \Phi_0 \cdot \begin{cases} \left(\frac{N-aA}{bA}\right)^{-\gamma} \\ \left(\frac{N+C-aB}{bB}\right)^{-\gamma} \end{cases} \quad \Rightarrow N \cdot (\log \Phi)' = \begin{cases} \frac{-\gamma N}{N-aA} \\ \frac{-\gamma N}{N+C-aB} \end{cases}$$

A change in slope occurs at $N_{ch,0}$ corresponding to $E_{i,0} = (e^{bh} - 1) \cdot a/b$ which depends only on the geometrical configuration of the detector. Therefore, the number of events with N_{ch} above $N_{ch,0}$ can be used to get the total flux above $E_{i,0}$, i.e. to find the normalization constant Φ_0.

At this N_{ch} the slope $N \cdot (\log \Phi)'$ (to the right or left) is proportional to γ. It can also be seen that it does not depend on the OM sensitivities/ice properties, since ρ cancels out.

Model of the N_{ch} behavior at small N_{ch}

To evaluate per event energy loss in the detector, a standard Monte Carlo chain consisting of only dCORSIKA and MMC was run. Detector was assumed to have radius of 125 meters and length of 400 meters. A "-user" option was used to record muon energy when entering and leaving (if leaving) the active volume of the detector, which then allowed to calculate the total energy deposited by all muons in the event inside the active volume of the detector. From the discussion above, this energy is proportional to N_{ch}.

Model of the N_{ch} behavior at small N_{ch}

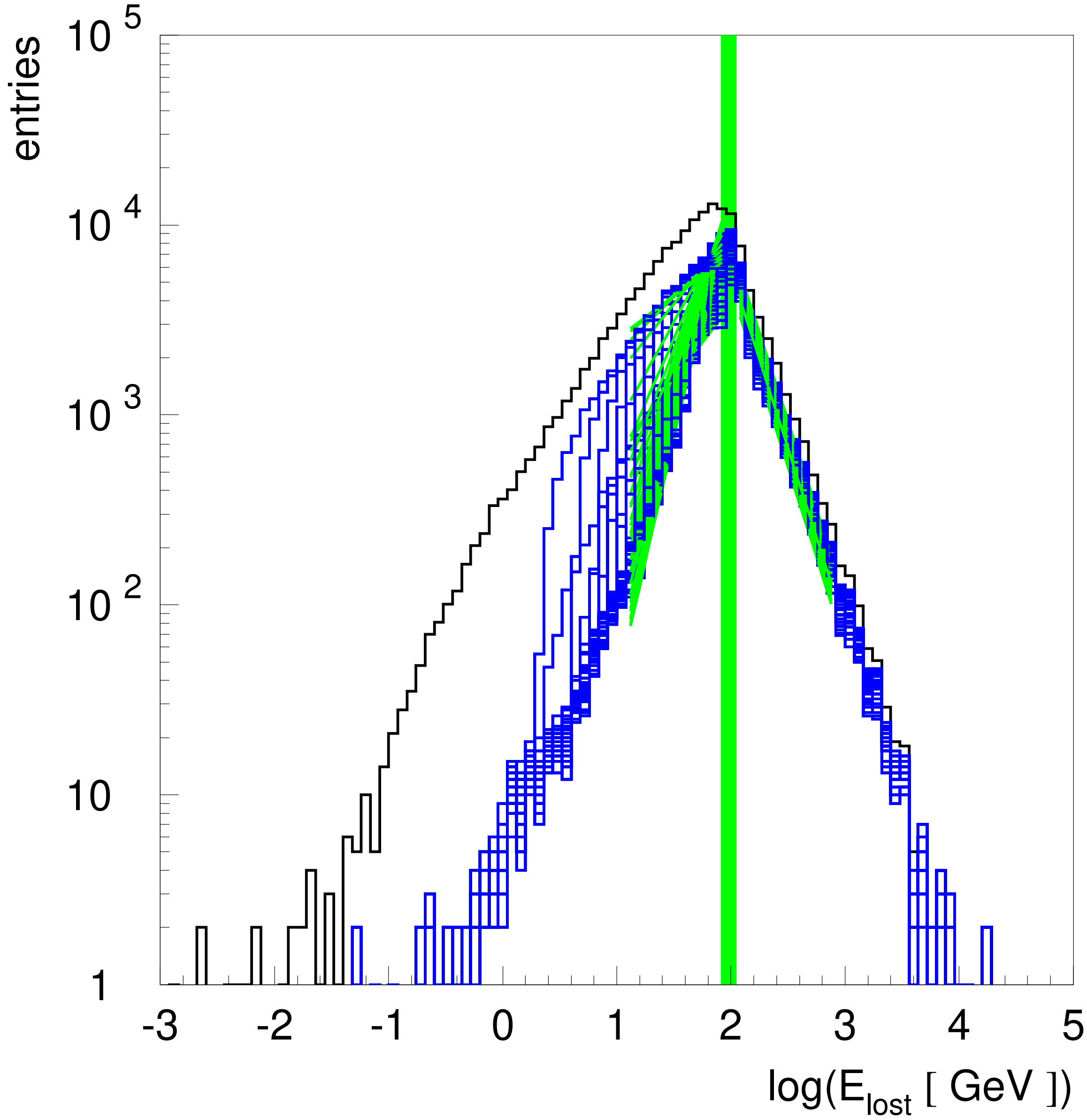

For each layer inside the detector (z-coordinates -200 through 200) energy lost by muons is histogrammed if at least one muon from the bundle reaches that layer. The distributions are found to follow the broken spectrum discussed above, and the maxima (corresponding to the braking point) are found and denoted by green lines.

Model of the N_{ch} behavior at small N_{ch}

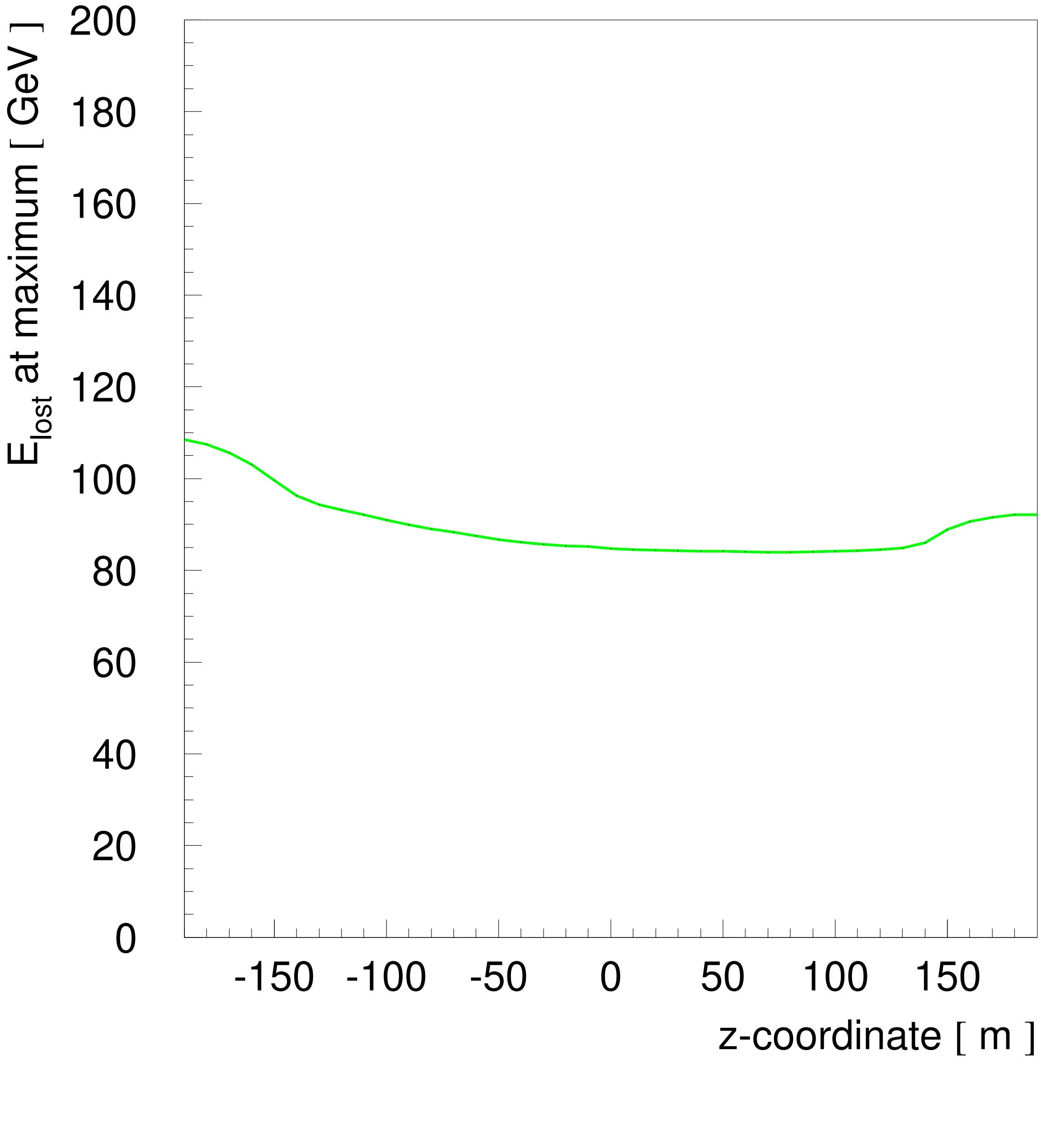

Energy for muons reaching given z-coordinate corresponding to the breaking point E_{ns} in the $N_{ch} \propto E_{lost}$ distribution depends weakly on the depth and is roughly 85-90 GeV.

Model of the N_{ch} behavior at small N_{ch}

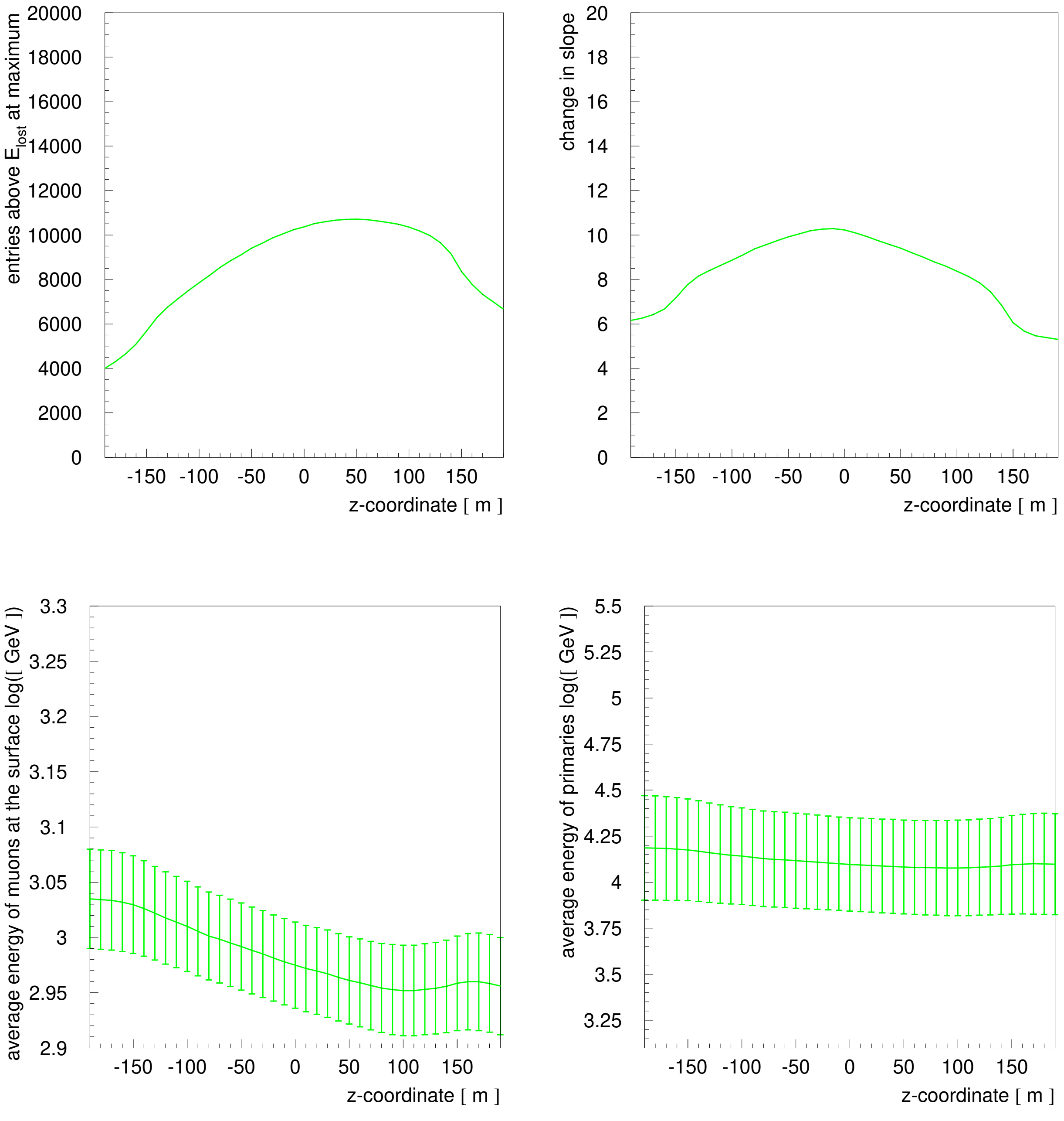

Energy of a typical muon loosing energy E_{ns} inside the active volume of the detector is about 1 TeV, and energy of a typical primary creating such a muon is about 14 TeV.

Fits for smaller energy E_{ns} (N_{ch})

Same as above, except N_{ch} is replaced with $\log(N_{ch})$, i.e. the new function is $g(x) = f(\log(x))$. To make the fit more stable only first exponent is left in $f(x)$.

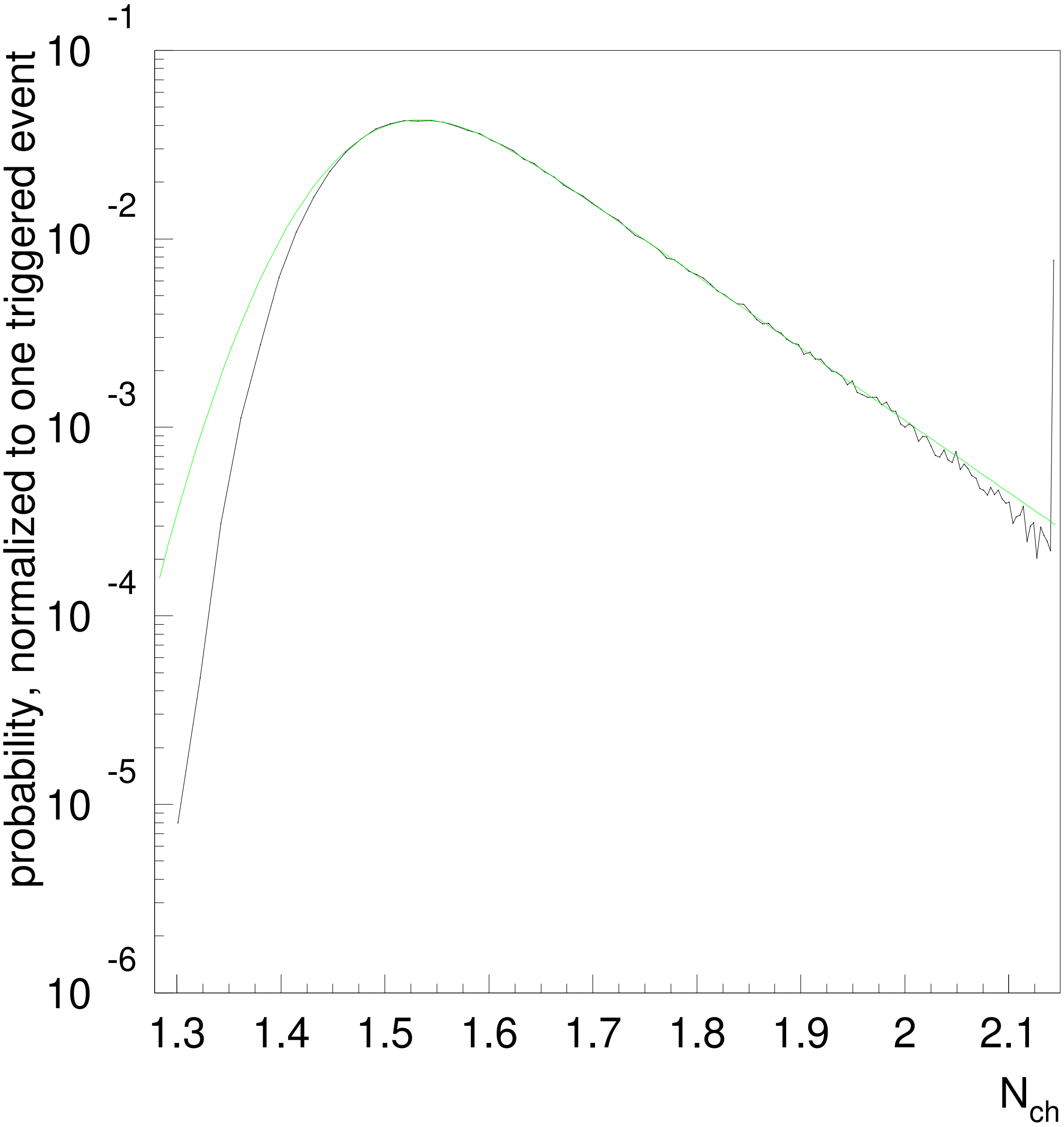

Fits for smaller energy E_{ns} (N_{ch})

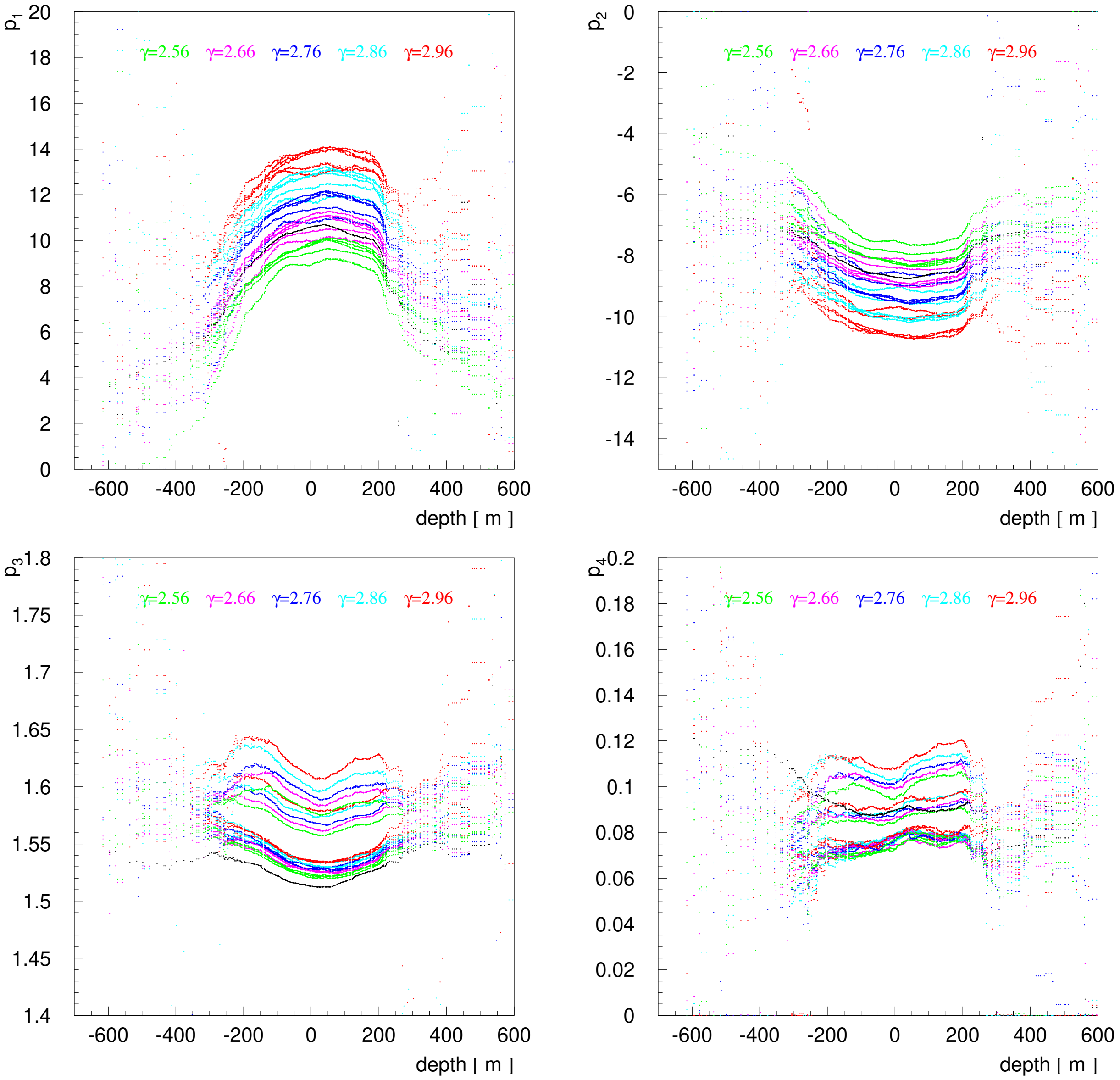

p_1 can be used for normalization, and p_2 for spectral index determination. p_3 is apparently correlated with both p_1 and p_2 and can be used to bring the curves in p_1 and p_2 plots closer together for each spectral index correction. p_4 does not exhibit consistent behavior from one ice model to another, and is avoided in the following analysis.

Spectral index determination at small N_{ch}

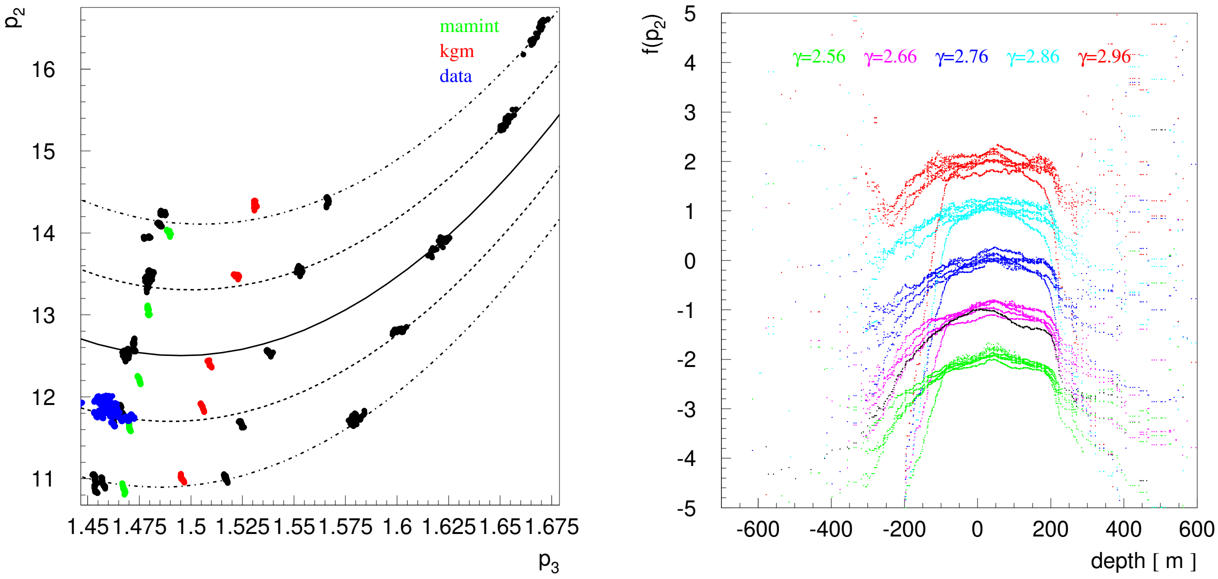

Log of normalization at small N_{ch}

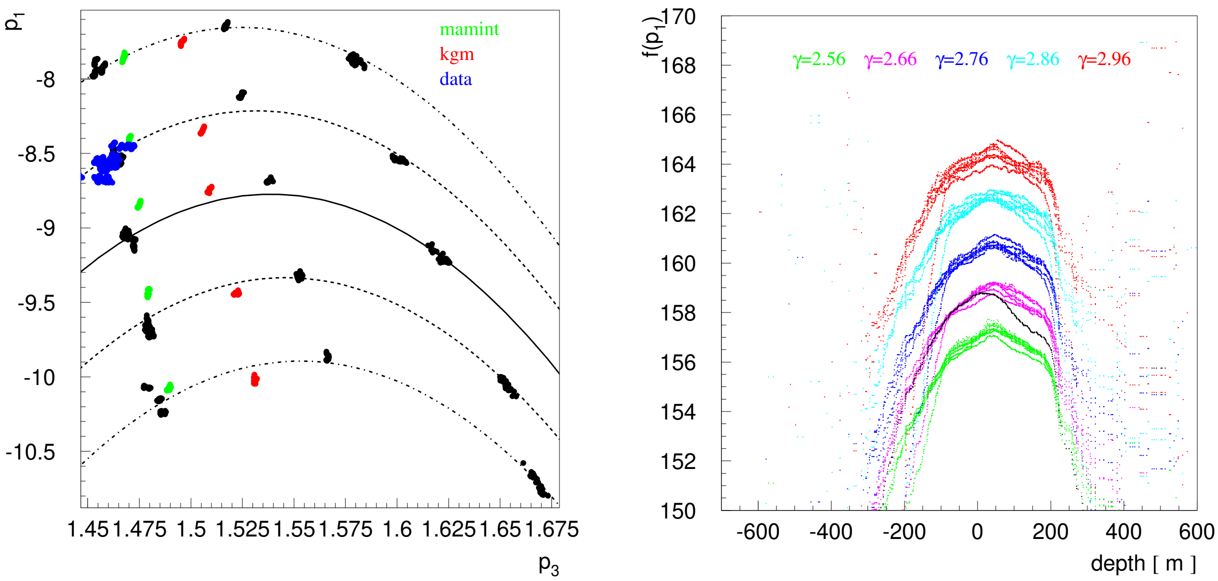

correlation with p_3 index and normalization

Conversion to spectral index correction coordinates

spectral index correction

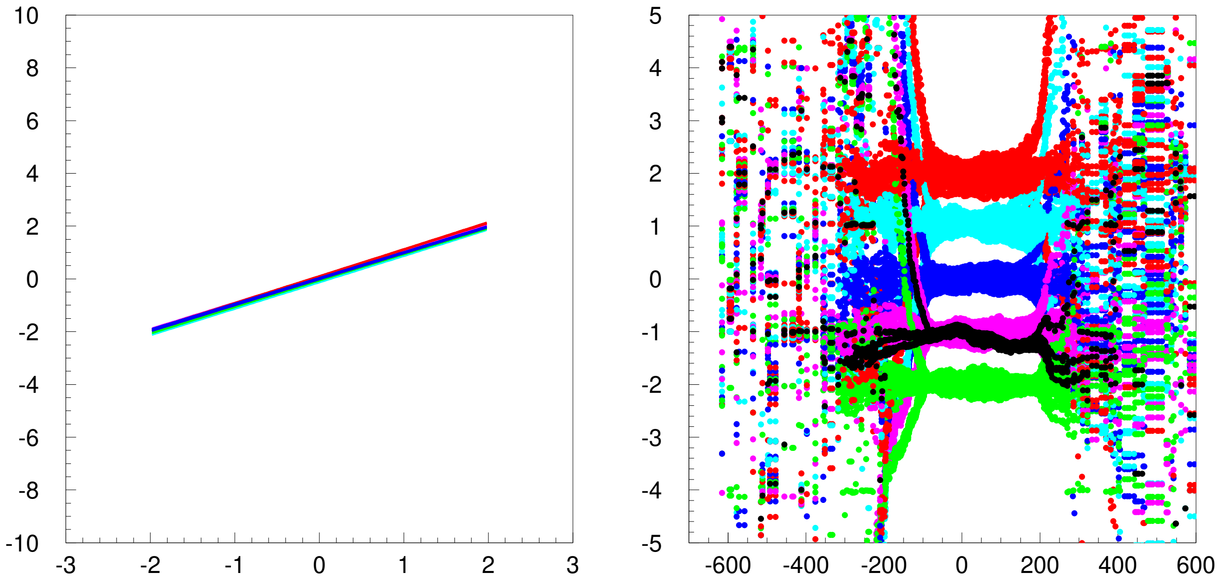

normalization correction

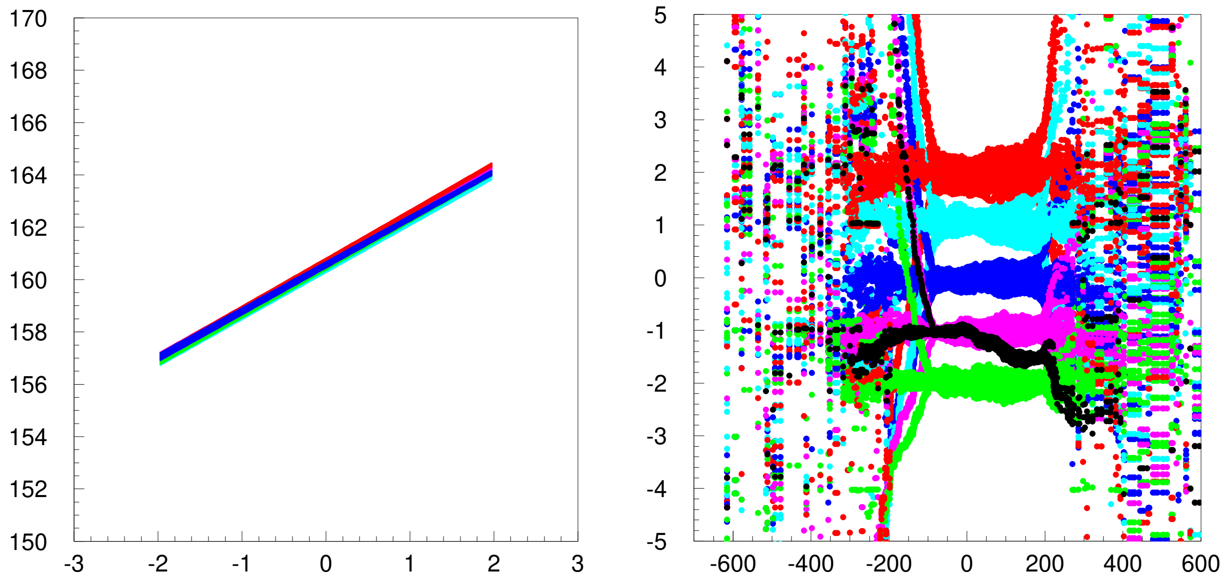

conversion function

converted plots

Results: 1st method, spectral index correction

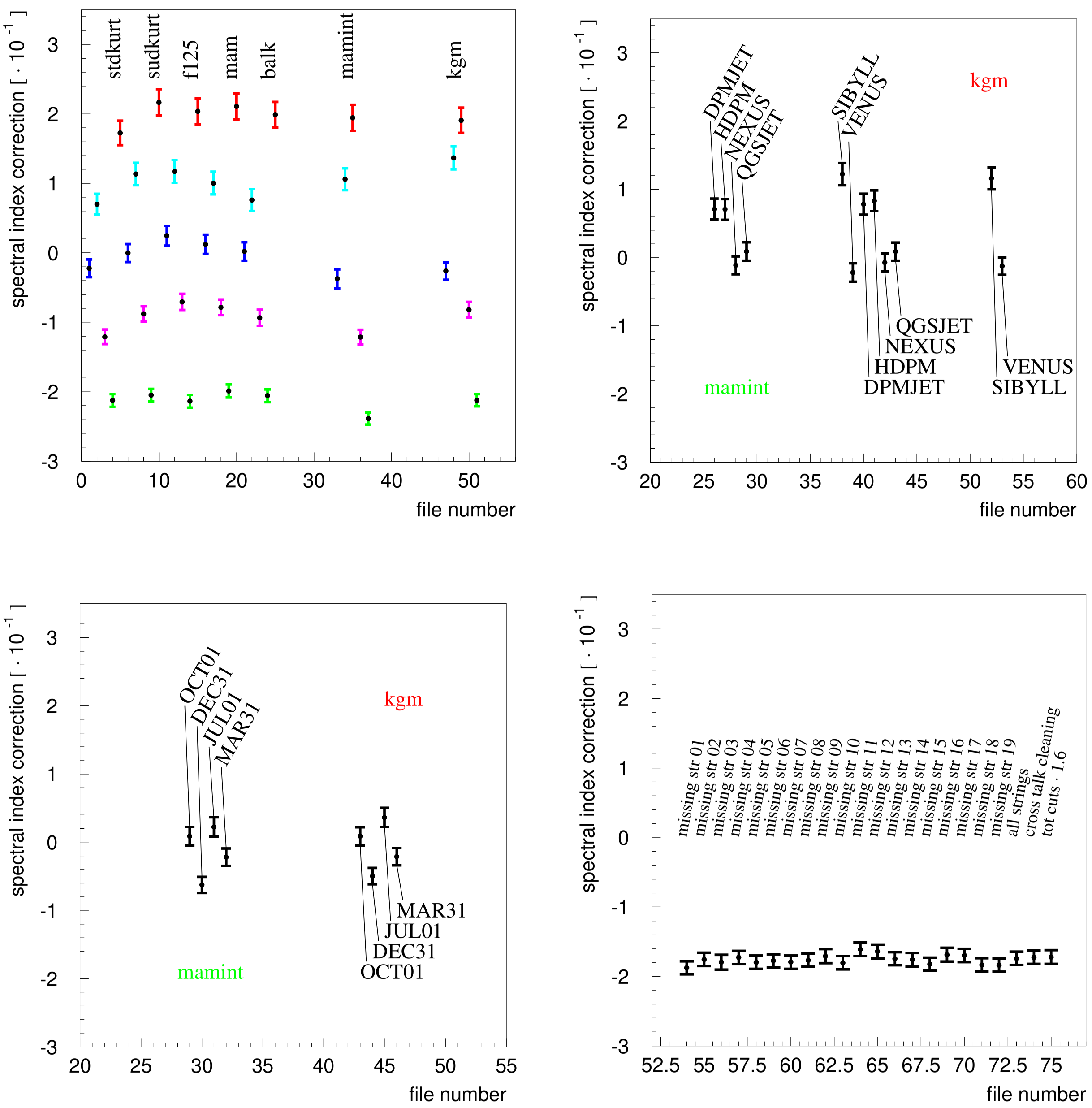

For QGSJET, day 55 (about halfway between DEC31 and MAR31),

$$\gamma = 2.76 + (-1.72 \pm 0.10 + 0.47 \pm 0.13(atm)) \cdot 10^{-1} = 2.64 \pm 0.02 \text{ (H component)}$$

Results: 1st method, normalization correction

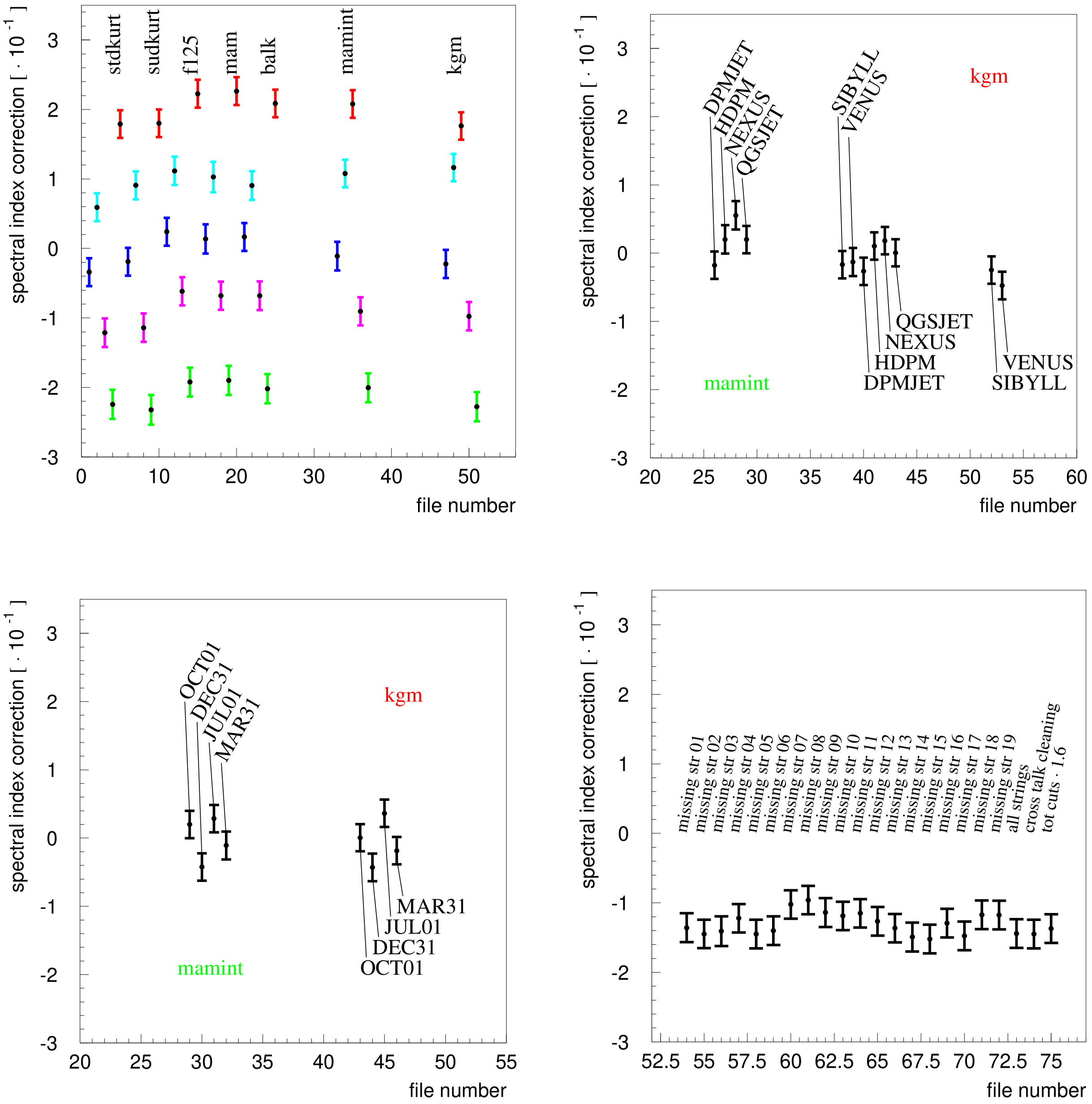

$$\Phi_0 = 0.1057(H) \cdot 10^{-0.19(conversionslope)\cdot(-1.45\pm0.21+0.39\pm0.20(atm)+0.75\pm0.23(\gamma\ correction))}$$

$$\Phi_0 = 0.1057 \cdot 10^{0.059\pm0.122}$$

Results: 2st method, spectral index correction

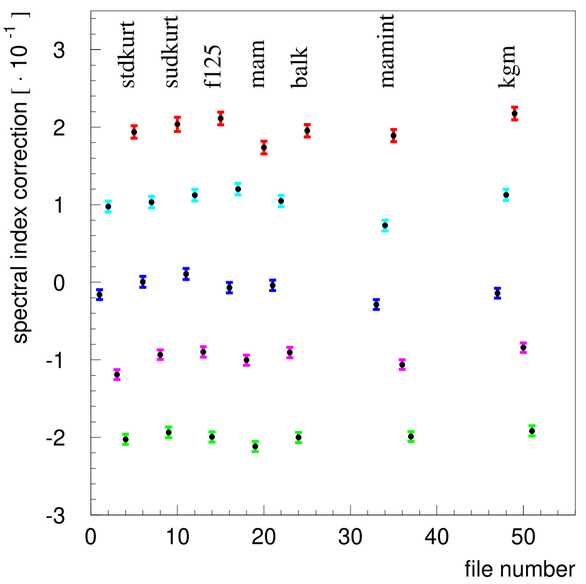

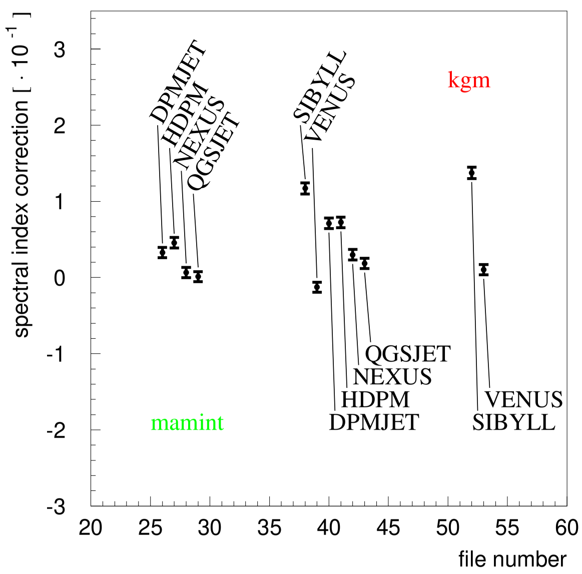

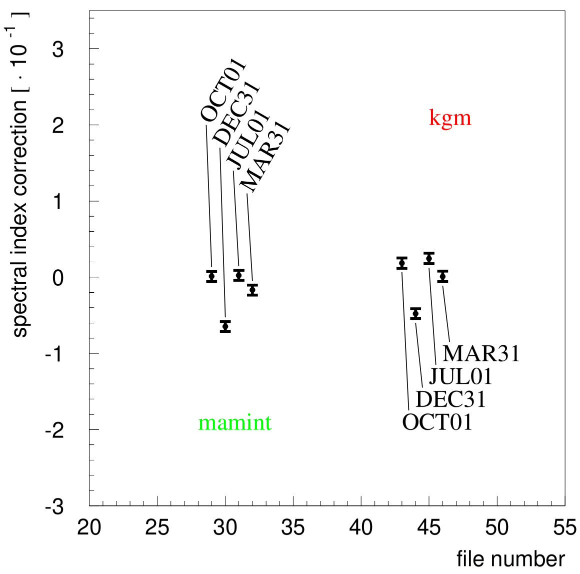

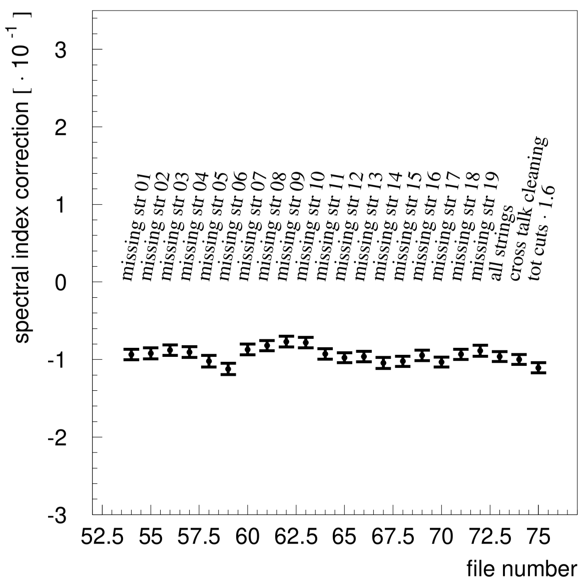

For QGSJET, day 55 (about halfway between DEC31 and MAR31),

$\gamma = 2.76 + (-1.00 \pm 0.06 + 0.42 \pm 0.07(atm)) \cdot 10^{-1} = 2.70 \pm 0.01$ (H component)

Results: 2st method, normalization correction

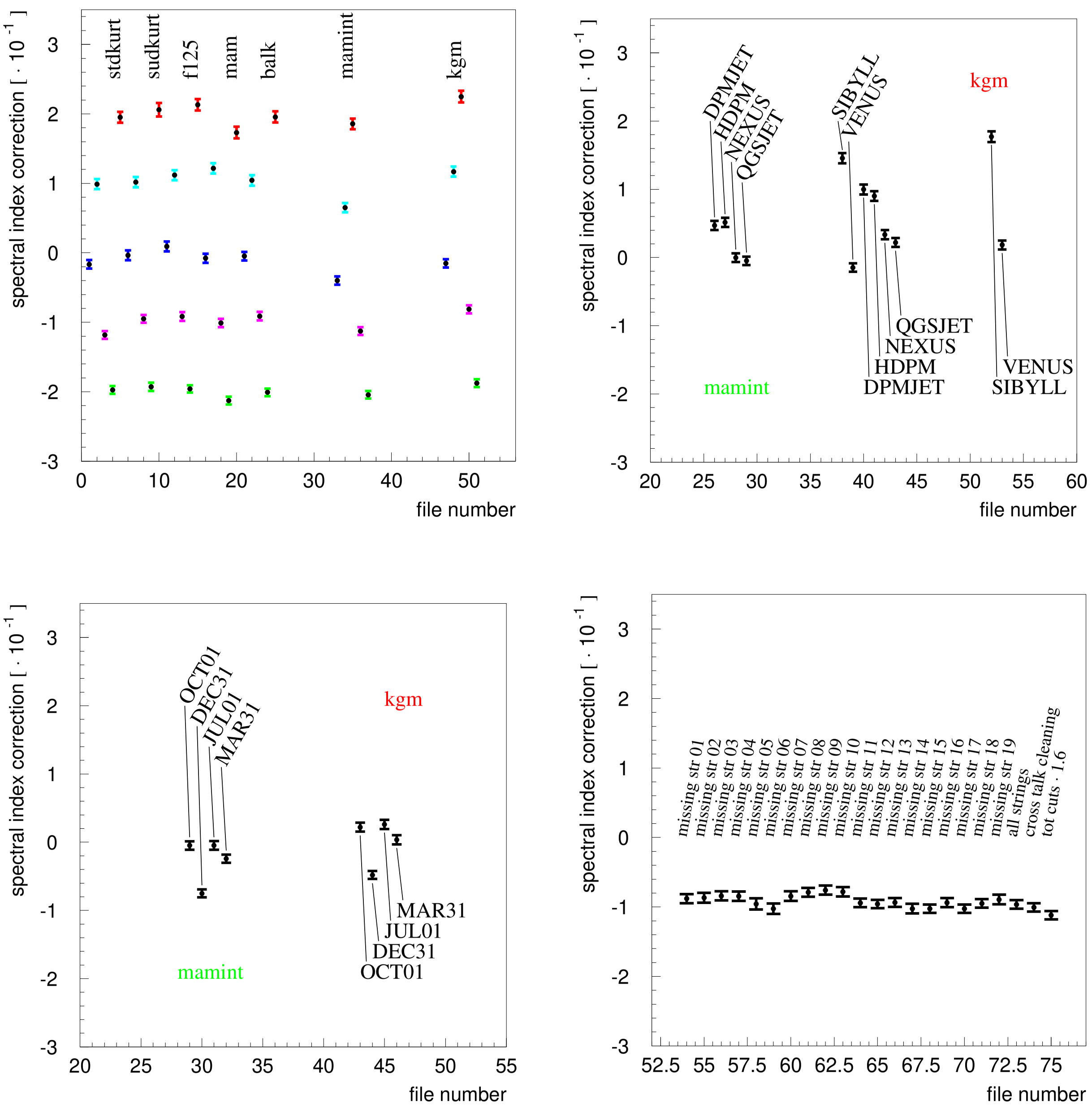

$$\Phi_0 = 0.1057(H)\cdot 10^{\log_{10}(e)\cdot 1.75(conversionslope)\cdot(-1.01\pm0.06+0.45\pm0.06(atm)+0.58\pm0.13(\gamma\ correction))}$$

$$\Phi_0 = 0.1057\cdot 10^{0.015\pm0.190}$$

Conclusions

1. Method presented in Part 1 (Zeuthen) was improved by better describing the cutoff at small N_{ch}, which stabilized the fits.

2. In addition to the high N_{ch} part of the N_{ch} distribution used before, a low N_{ch} part corresponding to lower muon energies can be used. This allows to get spectral index and normalization for another region of energies (1 TeV vs. 2 TeV).

3. Calculation for 6 different high-energy models (all now available in CORSIKA: QGSJET, SIBYLL, VENUS, DPMJET, NEXUS, and HDPM) and 4 different atmospheres was done. Ice models processed are mamint, kgm, stdkurt, sudkurt, f125, mam, and bulk.

4. Spectral index resolution due to systematic errors (ice model and detector configuration) is good enough to separate different high energy models. Although none of the models describe the data perfectly, QGSJET, VENUS and NEXUS seem to fit the data best.